

Evolution of Coherence and Superconductivity in Electron-Doped Cuprates

M. M. Qazilbash^{1,2}, B. S. Dennis¹, C. A. Kendziora³, Hamza Balci², R. L. Greene², and G. Blumberg^{1,†}

¹*Bell Laboratories, Lucent Technologies, Murray Hill, NJ 07974*

²*Center for Superconductivity Research, Department of Physics,
University of Maryland, College Park, MD 20740*

³*United States Naval Research Laboratory, Code 6365, Washington D.C. 20375*

(Dated: March 23, 2022)

The electron-doped cuprates were studied by electronic Raman spectroscopy across the entire region of the superconducting (SC) phase diagram. We determined that the magnitude of the SC order parameter varies between 4.6 and 3.5 $k_B T_c$, consistent with weak coupling BCS theory. Using a “Raman conductivity” sum rule, we found that doped carriers divide into coherent quasi-particles (QPs) and carriers that remain incoherent. The coherent QPs mainly reside in the vicinity of $(\pm\pi/2a, \pm\pi/2a)$ regions of the Brillouin zone. The carriers doped beyond optimal doping remain incoherent. Only coherent QPs contribute to the superfluid density in the SC state.

PACS numbers: 74.25.Gz, 74.72.Jt, 78.30.-j

Introduction.— In recent years, there has been renewed interest in the physical properties of electron n -doped high T_c superconducting (SC) cuprates. While there is considerable evidence that the SC order parameter (OP) of the hole p -doped cuprates has d -wave symmetry in the entire doping range of their SC phase [1, 2], the situation for the n -doped compounds still remains controversial. Earlier Raman data for optimally-doped (OPT) samples implied a non-monotonic d -wave OP [3]. There is disagreement among the few experiments that have studied the doping dependence of the SC OP [4, 5, 6, 7]. Angle-resolved photoemission spectroscopy (ARPES) data at optimal doping indicates the presence of both well-defined quasi-particles (QPs), as well as ill defined incoherent excitations [8]. There is current interest in examining the relationship between the coherence properties of introduced carriers and development of the SC OP with doping. We report a systematic low energy electronic Raman spectroscopy (ERS) study of $\text{Pr}_{2-x}\text{Ce}_x\text{CuO}_{4-\delta}$ (PCCO) and $\text{Nd}_{2-x}\text{Ce}_x\text{CuO}_{4-\delta}$ (NCCO) single crystals and films with different cerium doping covering the entire SC region of the phase diagram and determine the magnitude of the OP as a function of doping. By applying a “Raman conductivity” sum rule [9, 10], we find that carriers doped beyond optimal doping remain incoherent and do not contribute to the superfluid density.

Experimental.— Raman scattering was performed from natural ab surfaces of single crystals and films of PCCO and single crystals of NCCO. Crystals with different Ce concentrations were grown using a flux method as described in [11]. After growth, the crystals were annealed in an Ar-rich atmosphere to induce superconductivity. The SC transitions were measured by a SQUID magnetometer. The Ce concentration of the crystals was measured with wavelength dispersion spectroscopy. c -axis oriented PCCO films were grown on strontium titanate substrates using pulsed laser deposition [12]. The films were grown to a thickness of about 0.8 to 1 μm to min-

imize the substrate contribution to the Raman signal. The SC transitions were measured by ac susceptibility. The films provide an opportunity to study the extremes of the SC phase because of better control of Ce doping in under-doped (UND) and highly over-doped (OVD) samples.

The samples were mounted in an optical continuous helium flow cryostat. The spectra were taken in a pseudo-backscattering geometry using linearly polarized excitations at 647 and 799 nm from a Kr^+ laser. Incident laser powers between 0.5 and 4 mW were focused to a $50 \times 100 \mu\text{m}$ spot on the sample surface. The spectra were measured at temperatures between 4 and 30 K by a custom triple grating spectrometer and the data were corrected for instrumental spectral response. The sample temperatures quoted in this work have been corrected for laser heating.

Raman scattering symmetries.— The polarization directions of the incident, \mathbf{e}_i , and scattered, \mathbf{e}_s , photons are indicated by $(\mathbf{e}_i\mathbf{e}_s)$ with $x=[100]$, $y=[010]$, $x'=[110]$ and $y'=[\bar{1}10]$. The presented data were taken in (xy) , $(x'y')$ and (xx) scattering geometries. For the tetragonal D_{4h} symmetry of the n -doped cuprates, these geometries correspond to $B_{2g}+A_{2g}$, $B_{1g}+A_{2g}$ and $A_{1g}+B_{1g}$ representations. Using circularly polarized light we confirmed that the contribution to the A_{2g} channel is very weak for both PCCO and NCCO.

The electronic Raman response function, $\chi''^{(is)}(\omega)$, for a given polarization geometry $(\mathbf{e}_i\mathbf{e}_s)$ is proportional to the sum over the density of states at the Fermi surface (FS) weighted by the square of the momentum \mathbf{k} dependent Raman vertex $\gamma_{\mathbf{k}}^{(is)}$ [13, 14, 15]. Because the scattering geometries selectively discriminate between different regions of the FS, ERS provides information about both the magnitude and the \mathbf{k} dependence of the SC OP. In the effective mass approximation $\gamma_{\mathbf{k}}^{B_{1g}} \propto t(\cos k_x a - \cos k_y a)$ and $\gamma_{\mathbf{k}}^{B_{2g}} \propto 4t'(\sin k_x a \sin k_y a)$ where t and t' are nearest and next-nearest neighbor hopping integrals in the

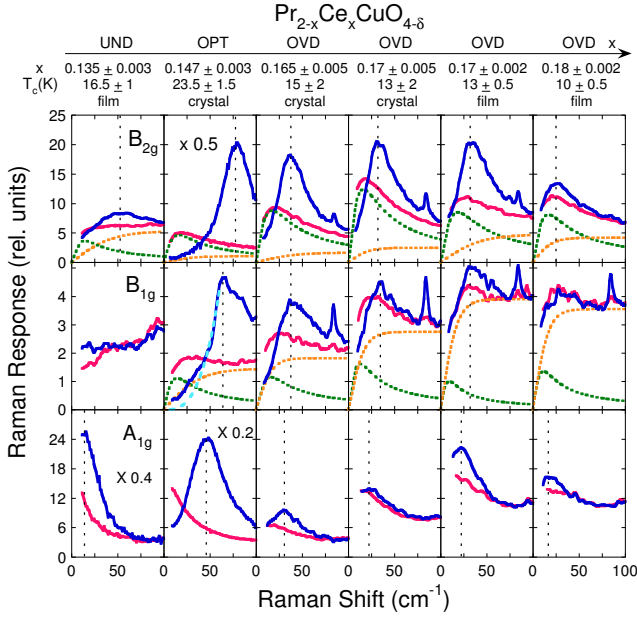


FIG. 1: Doping dependence of the low energy electronic Raman response of PCCO single crystals and films for B_{2g} , B_{1g} and A_{1g} channels obtained with 647 nm excitation. The columns are arranged from left to right in order of increasing cerium doping. The light (red) curves are the data taken just above the respective T_c of the samples. The normal state response in the B_{2g} and B_{1g} channels is decomposed into a coherent Drude contribution in a quasi-elastic form (green dotted line) and an incoherent continuum (yellow dotted line). The dark (blue) curves show the data taken in the SC state at $T \approx 4$ K. The dashed vertical lines indicate positions of the 2Δ peak. For the OPT crystal a low-frequency ω^3 power law is shown in the B_{1g} panel for comparison (light-blue dotted line). OVD crystals and films show similar behavior, indicating the good quality of the films.

tight-binding model. For the B_{2g} channel the Raman vertex is maximum around $(\pi/2a, \pi/2a)$ and equivalent regions of the Brillouin zone (BZ) and vanishes along $(0, 0) \rightarrow (\pi/a, 0)$ and equivalent lines. For the B_{1g} channel nodal $(0, 0) \rightarrow (\pi/a, \pi/a)$ diagonals do not contribute to the intensity that mainly integrates from the regions near intersections of the FS and the BZ boundary.

Figure 1 exhibits the evolution with doping of the Raman response function above T_c and at 4 K, deep in the SC state, for all three observable symmetry channels: B_{2g} , B_{1g} and A_{1g} . The total intensity is significantly stronger in the B_{2g} than in the B_{1g} channel for all doping concentrations. This underlines the importance of the next-nearest neighbor hopping t' for the n -doped cuprates and is in contrast with p -doped cuprates where the response in the B_{2g} channel is generally weaker than in B_{1g} [16]. Although Coulomb screening should lead to a much weaker Raman response in the fully symmetric channel, we find that the intensities in the A_{1g} channel are of the same order of magnitude as those in crossed

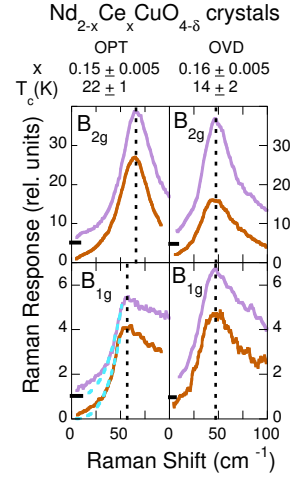


FIG. 2: A comparison of the Raman response in the SC state for OPT (first column) and OVD (second column) NCCO crystals. The first and second rows show spectra for B_{2g} and B_{1g} channels respectively. The violet (light) and orange (dark) curves are data taken with red laser excitation ($\lambda_L = 647$ nm) and near-IR excitation ($\lambda_L = 799$ nm). The B_{2g} and B_{1g} data for $\lambda_L = 647$ nm has been shifted up by 5 units and 1 unit respectively. All spectra are taken at $T \approx 4$ K. The dashed vertical lines show the positions of the 2Δ peaks. For the OPT crystal a low-frequency ω^3 power law is shown in the B_{1g} panel for comparison (light-blue dotted line).

polarizations in the OVD samples and are significantly stronger in the UND and OPT samples. This lack of screening is not understood within the framework of existing theoretical models.

Pair breaking excitations out of the SC condensate.— In the B_{2g} and A_{1g} channels, the pair-breaking 2Δ coherence peaks appear for all doping concentrations while in the B_{1g} channel the 2Δ peaks are negligibly weak in the UND and the most OVD films. For the OPT crystal ($T_c = 23.5$ K) the coherence peak energy is larger for the B_{2g} channel compared with that in B_{1g} and for all channels it is larger than the scattering rate Γ obtained from the spectra in the normal state discussed in the following section. The intensity below the coherence peaks vanishes smoothly without a threshold to the lowest frequency measured. The absence of a threshold that has been observed in s -wave superconductors precludes interpretation in terms of a fully gapped Fermi surface [13]. The smooth decrease in the Raman response below the 2Δ peak is consistent with nodes in the gap. We compare the low-frequency tail in the B_{1g} response (Fig. 1) to an ω^3 power law that is expected for a $d_{x^2-y^2}$ -wave superconductor in the clean limit [17]. The observed deviation from cubic to a linear response at the lowest frequencies is an indication of low-energy QP scattering [18, 20]. The data for OPT PCCO is very similar to that for OPT NCCO (see Fig. 2) which was interpreted in terms of a non-monotonic d -wave order parameter with nodes along

the $(0, 0) \rightarrow (\pi/a, \pi/a)$ diagonal and the maximum gap being closer to this diagonal than to the BZ boundaries [3].

Interestingly, in the OVD PCCO samples (Fig. 1) and OVD NCCO crystal (Fig. 2), the 2Δ peak positions are at the same energies for both the B_{2g} and B_{1g} channels. The 2Δ peak positions and intensities decrease in the OVD regime compared to the OPT samples. Moreover, $2\Delta \sim \Gamma$ indicates that superconductivity is approaching the dirty or disordered limit [20]. The Raman response below the 2Δ -peaks vanishes smoothly and no well-defined threshold is observed. The data for the 799 nm excitation is measured down to 4.5 cm^{-1} and shows no obvious sub-gap threshold. The peak positions and the sub-gap Raman response in the NCCO crystals are almost independent of the laser excitation energies (Fig. 2). A similar symmetry independent pair breaking peak energy with continuously decreasing Raman scattering intensity down to the lowest frequencies measured has been observed in the Raman spectra in OVD samples of p -doped Bi-2212 [21]. The Raman data presented in Figs. 1-2 for OVD n -doped samples is similar to the Raman data for OVD Bi-2212. The coincidence of the coherence peak energies in the B_{1g} and B_{2g} channels is probably caused by enhanced QP scattering [20]. Nevertheless, the continuously decreasing Raman intensity below the coherence peak is not inconsistent with a nodal gap structure.

Figure 3(a) summarizes the energy of the 2Δ coherence peak as a function of doping for all three scattering channels. The coherence peak energy has a pronounced maximum at optimal doping. The 2Δ features in the A_{1g} channel occur at lower energies compared to those in the B_{2g} and B_{1g} channels. For comparison, we include the value of twice the SC gap energy obtained from point contact tunneling spectroscopy [22]. While for OPT and OVD samples the maximum value of the Raman 2Δ peak positions are very similar to the single particle spectroscopy gap values, this is not the case for the UND samples where the tunneling spectroscopy data exhibits a gap that is larger than the Raman coherence peaks. For UND samples the two QPs excited out of the SC condensate by Raman processes continue to interact, binding into a collective excitonic state that costs less energy than excitation of two independent QPs. Similar observations were made previously for p -doped cuprates [16, 23]. The importance of the final state interactions in the formation of a collective mode in UND cuprates has been demonstrated in Refs. [24, 25].

Reduced energies of the coherence peaks, $2\Delta/k_B T_c$, are plotted in Fig. 3b as a function of doping. For the channel that exhibits the highest ratio, B_{2g} , the values fall between 4.6 for the UND and OPT samples and 3.5 for the most OVD samples, within the prediction of the mean-field BSC values for d -wave superconductors [26]. The coherence peak energy remains below $4.2k_B T_c$ for

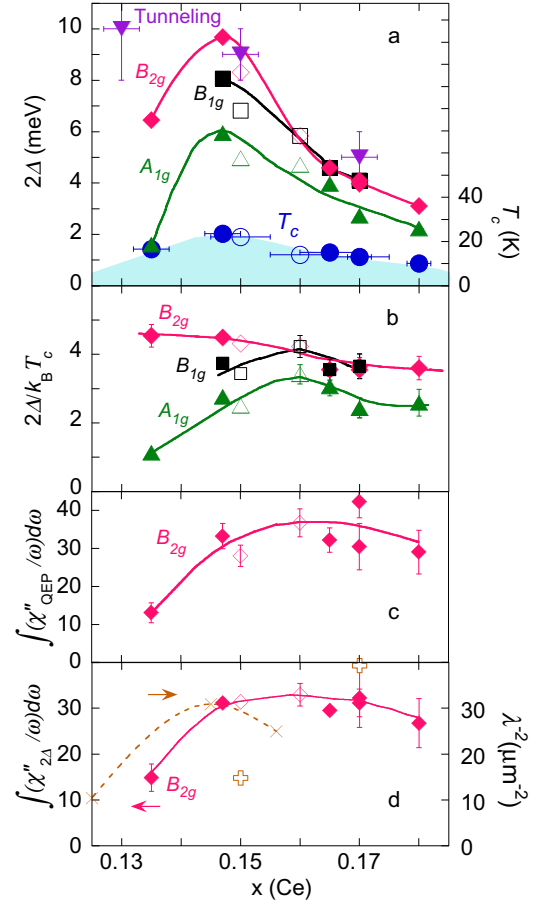


FIG. 3: The phase diagram of PCCO (filled symbols) and NCCO (open symbols) superconductors explored by ERS. Panels show: (a) T_c and 2Δ peak positions (gap magnitudes) for B_{1g} , B_{2g} and A_{1g} channels as well as the distance between coherence peaks from point contact tunneling spectroscopy [22]; (b) The magnitude of the reduced gap ($2\Delta/k_B T_c$) for three Raman channels; (c) The integrated QP (Drude) response just above T_c ; (d) The integrated intensity in the SC coherence peak at 4 K. For comparison, we plot $1/\lambda(0)^2$ values from refs. [5] (\times) and [7] (open crosses). Error bars on the cerium concentrations are shown only on the T_c data points to preserve clarity of the figure. Solid lines are guides to the eye.

the B_{1g} channel and is even lower for the A_{1g} channel, particularly for the UND sample. The reduced energies for all the channels are significantly lower than for p -doped materials [16, 23, 27] suggesting a BCS weak coupling limit for the n -doped cuprates.

Evolution with carrier doping in the normal state.— In the normal state the Raman response can be decomposed into a featureless continuum and a defined low-frequency quasi-elastic scattering peak (QEP): $\chi''_N(\omega) = \chi''_{QEP}(\omega) + \chi''_{MFL}(\omega)$. The QEP response $\chi''_{QEP}(\omega) = a^{(is)} \frac{\Gamma\omega}{\omega^2 + \Gamma^2}$ is described in a Drude model as a well defined QP contribution from doped carriers [10, 28] while the featureless continuum $\chi''_{MFL}(\omega) = b^{(is)} \tanh(\omega/\omega_c)$

represents a collective incoherent response [29]. Symmetry dependent $a^{(is)}$ and $b^{(is)}$ parameters control the spectral weight in these coherent and incoherent channels, ω_c is a cut-off frequency of order $k_B T$ [29] and the QEP position Γ is the Drude scattering rate that at low temperatures remains between 2 and 2.5 meV for the entire studied doping range. This deconvolution of the Raman response into two components presented here is consistent with the ARPES data that simultaneously displays defined QPs in the vicinity of the $(\pi/2a, \pi/2a)$ point and ill defined excitations in the other parts of the FS [8]. One can observe from the deconvolution that the Raman response in the B_{2g} channel is dominated by the QP (Drude) response while in the B_{1g} channel by the incoherent continuum [28, 30]. This confirms that the defined QP states reside in the vicinity of the $(\pm\pi/2a, \pm\pi/2a)$ regions of the BZ.

Figure 3(c) displays the evolution of the integrated QP spectral weight of the “Raman conductivity” [10] $I_N^{B_{2g}}(x) = \int (\chi_{QEP}''/ \omega) d\omega$ as a function of electron (Ce) doping x . While on the UND side $I_N^{B_{2g}}(x)$ exhibits the expected increase proportional to x , the integrated coherent contribution saturates above optimal doping $x \gtrsim 0.145$. At these higher concentrations, additional carriers contribute only to the incoherent response and can be observed as an increasing intensity of the featureless Raman continuum $\chi_{MFL}''(\omega)$, particularly in the B_{1g} channel (Fig. 1).

SC coherence peak intensity and sum rules.— In Fig. 3(d) we plot the integrated coherence intensity in the SC state, $I_{SC}^{B_{2g}}(x) = \int (\chi_{2\Delta}''/ \omega) d\omega$, where $\chi_{2\Delta}''(\omega)$ is the SC coherence response with the background subtracted. We note that the values of the integrated coherence intensity do not change from the normal to SC state (Fig. 3c and d) demonstrating a sum rule for the “Raman conductivity”. For the non-symmetric channels $I_{SC}^{(is)} \propto \sum_{\mathbf{k}} (\gamma_{\mathbf{k}}^{(is)})^2 \frac{\Delta_{\mathbf{k}}^2}{2E_{\mathbf{k}}^3}$ is proportional to the superfluid density $n_s \propto \sum_{\mathbf{k}} \frac{\Delta_{\mathbf{k}}^2}{2E_{\mathbf{k}}^3}$ weighted by the square of the Raman coupling vertex. Here $E_{\mathbf{k}}$ is the QP dispersion in the SC state. The superfluid densities ($n_s \propto 1/\lambda^2$) obtained from penetration depth (λ) measurements [5, 7] are plotted in Fig. 3(d) for comparison. The $I_N^{B_{2g}}(x) = I_{SC}^{B_{2g}}(x)$ equality implies that not all doped electrons but only Drude QPs control the superfluid density and that the incoherent carriers doped above optimal doping do not contribute to the superfluid stiffness [31].

Summary.— ERS has been investigated across the entire SC phase diagram of the n -doped cuprates. The SC gap magnitude has a maximum near optimal doping. The gaps measured by ERS are in agreement with those measured by single particle spectroscopy for OPT and OVD samples. For the UND film, the Raman data shows a smaller gap implying strong final state interactions. The reduced coherence peak values ($2\Delta/k_B T_c$) for the B_{2g}

channel decrease monotonically from 4.6 for the UND sample to 3.5 for OVD samples. Using the “Raman conductivity” sum rule, we find that carriers doped beyond optimal doping remain incoherent and do not contribute to the Drude conductivity and superfluid density. The reduced ratio of coherent on the background of incoherent carriers possibly explains the fragility of superconductivity in the OVD n -doped cuprates.

The authors thank A. Koitzsch, A. Gozar, Y. Dagan, C. P. Hill and M. Barr for assistance, B. Liang for WDS measurements, V. N. Kulkarni for Rutherford Backscattering on PCCO films, and Z. Y. Li for crystal growth. This work was supported in part by NSF Grant No. DMR 01-02350.

-
- [†] E-mail: girsh@bell-labs.com
 - [1] D. van Harlingen, Rev. Mod. Phys. **67**, 515 (1995).
 - [2] C. C. Tsuei and J. R. Kirtley, Rev. Mod. Phys. **72**, 969 (2000).
 - [3] G. Blumberg *et al.*, Phys. Rev. Lett. **88**, 107002 (2002); Phys. Rev. Lett. **90**, 149702 (2003).
 - [4] A. Biswas *et al.*, Phys. Rev. Lett. **88**, 207004 (2002).
 - [5] J. A. Skinta *et al.*, Phys. Rev. Lett. **88**, 207005 (2002).
 - [6] M. Kim *et al.*, Phys. Rev. Lett. **91**, 087001 (2003).
 - [7] A. Snezhko *et al.*, Phys. Rev. Lett. **92**, 157005 (2004).
 - [8] N. P. Armitage *et al.*, Phys. Rev. Lett. **88**, 257001 (2002); T. Claesson *et al.*, Phys. Rev. Lett. **93**, 136402 (2004).
 - [9] B. S. Shastry, and B. I. Shraiman, Phys. Rev. Lett. **65**, 1068 (1990).
 - [10] G. Blumberg and M. V. Klein, J. of Low. Temp. Phys. **117**, 1001 (1999).
 - [11] J. L. Peng *et al.*, Physica C **177**, 79 (1991).
 - [12] E. Maiser *et al.*, Physica C **297**, 15 (1998).
 - [13] S.B. Dierker *et al.*, Phys. Rev. Lett. **50**, 853 (1983); R. Hackl *et al.*, J. Phys. C **16**, 1729 (1983).
 - [14] M. V. Klein and S. B. Dierker, Phys. Rev. B **29**, 4976 (1984).
 - [15] T. P. Devereaux and D. Einzel, Phys. Rev. B **51**, 16336 (1995).
 - [16] H. L. Liu *et al.*, Phys. Rev. Lett. **82**, 3524 (1999).
 - [17] T. P. Devereaux *et al.*, Phys. Rev. Lett. **72**, 396 (1994).
 - [18] Optical conductivity data also indicates that OPT PCCO films are between the clean and dirty limits [19].
 - [19] A. Zimmers *et al.*, cond-mat/0405284.
 - [20] T. P. Devereaux *et al.*, Phys. Rev. Lett. **74**, 4313 (1995).
 - [21] C. Kendziora *et al.*, Phys. Rev. Lett. **77**, 727 (1996); R. Hackl *et al.*, SPIE (Bellingham) Vol. **2696**, 194 (1996); T. Masui *et al.*, Phys. Rev. B **68**, 060506(R) (2003).
 - [22] M. M. Qazilbash *et al.*, Phys. Rev. B **68**, 024502 (2003).
 - [23] G. Blumberg *et al.*, Science **278**, 1427 (1997); J. Phys. Chem. Solids **59**, 1932 (1998).
 - [24] A. Bardasis and J. R. Schrieffer, Phys. Rev. **121**, 1050 (1961).
 - [25] A.V. Chubukov, D.K. Morr and G. Blumberg, Solid St. Comm. **112**, 183 (1999).
 - [26] H. Won and K. Maki, Phys. Rev. B **49**, 1397 (1994).
 - [27] C. Kendziora and A. Rosenberg, Phys. Rev. B **52**, 9867 (1995).

- [28] A. Koitzsch *et al.*, Phys. Rev. B **67**, 184522, (2003).
- [29] C. M. Varma, Phys. Rev. Lett. **63**, 1996 (1989).
- [30] The featureless continuum is stronger for the film samples compared to the single crystals. This is an indication of additional disorder and/or possible strain fields.
- [31] The above analysis assumes that the resonant properties of the Raman vertex, i.e. the optical conductivity near the laser excitation of 647 nm (1.9 eV), do not change with doping in the relevant doping range ($0.13 < x < 0.18$). Indeed, there is only a weak change in optical conductivity above 0.8 eV with doping in the relevant doping range [32].
- [32] T. Arima *et al.*, Phys. Rev. B **48**, 6597 (1993); Y. Onose *et al.*, Phys. Rev. B **69**, 024504 (2004).